On the Use of Rotating Hydraulic Models

K. M. BORENÄS AND L. J. PRATT

Department of Physical Oceanography, Woods Hole Oceanographic Institution, Woods Hole, Massachusetts

(Manuscript received 27 May 1992, in final form 21 April 1993)

ABSTRACT

Two problems regarding the use of rotating hydraulic channel flow models are addressed. The first concerns the difficulties encountered when trying to identify the "potential" depth for a flow of uniform (but nonzero) potential vorticity in a practical situation. Guidelines are given to check whether a chosen value of the potential depth is consistent with the rotating hydraulic theory. The second problem deals with the applicability of the so-called zero potential vorticity approximation. It is shown that the accuracy of this approximation depends on the ratio of the channel width to the Rossby radius of deformation (based on the potential depth) and the ratio of the fluid depth to the potential depth. To establish when this simplified model yields an accurate approximation of a flow of constant (but nonzero) potential vorticity, the two models are compared for a variety of channel geometries.

1. Introduction

Rotating hydraulic theory has been used a number of times to estimate the maximum possible deep mass transport through passages in the ocean (see Whitehead et al. 1974; Whitehead 1986; Borenäs and Lundberg 1988). In these models, the potential vorticity is usually taken to be uniform and defined by

$$\frac{f+\xi}{D} = \frac{f}{D_\infty}. \tag{1}$$

Here f, ξ, and D represent the Coriolis parameter, relative vorticity, and fluid depth, respectively; D_∞, the "potential" depth, is the depth to which a particular column must be stretched in order to make $\xi = 0$, a condition often imagined to occur in the deep upstream reservoir or basin. [See Borenäs and Pratt (1990) and Pratt and Lundberg (1991) for a résumé of uniform as well as nonuniform potential vorticity flows.]

In the present investigation, two different problems concerning the practical use of the hydraulic models will be addressed. The first is whether the potential depth, D_∞, is a quantity that can be identified easily. It is usually assumed that in the main part of a very deep/broad upstream basin the velocity as well as the velocity shear is negligible. In the hydraulic models the potential depth is consequently taken to be identical to the fluid depth in the interior of the upstream basin. Whether a chosen value of the potential depth is consistent with the theory is examined by tracing the solutions into the reservoir and then comparing the typical fluid depth in the basin (generated by the model) with D_∞.

The second problem concerns the applicability of the approximation often referred to as the "zero potential vorticity" limit. If the right-hand side of Eq. (1) is small compared to both f/D and ξ/D, then it is possible to put $\xi \approx -f$ and solutions to the hydraulic problem are obtained in explicit form. The assumption that $f/D_\infty \ll f/D$ (or $D/D_\infty \ll 1$) has been called the deep reservoir limit (Pratt and Lundberg 1991). To assume that $f/D_\infty \ll \xi/D$ is equivalent to requiring that the channel width is much less than the Rossby radius of deformation based on the potential depth, D_∞. (The latter follows from a simple scaling argument involving the geostrophic relation.) This is the narrow channel limit (e.g., see Gill 1977).

An undesirable feature of the deep reservoir–narrow channel limit is that it is not uniformly valid. Although the approximation may hold over portions of the flow field, it may fail elsewhere. In particular, the model often predicts upstream features like large velocities, areas of strong recirculation, or a separated flow. For certain geometries the solutions may even cease to exist when traced upstream. To establish when the simplified model yields an accurate approximation of a flow of constant (nonzero) potential vorticity, the two models are compared for a variety of channel geometries.

The paper is organized in the following way. The equations for a flow of constant potential vorticity are presented in section 2. In section 3 the problem of identifying D_∞ is discussed. The simplified equations are derived in section 4, and in sections 5–6 their applicability is examined for two basic channel configurations. These are 1) a channel of constant depth that

Corresponding author address: Dr. Karin M. Borenas, Department of Oceanography, Göteborg University, Box 4038, S-400 40 Göteborg, Sweden.

widens upstream and 2) a channel of constant width that deepens upstream. The cross section of the channel is taken to be rectangular, but a comment will also be given for the case of a parabolic topography. A discussion of the results is given in section 7.

2. The governing equations for finite potential vorticity flow

The derivation of the governing equations closely follows that of Gill (1977). The shallow-water equations will be used for an inviscid fluid in a rotating system. In Fig. 1 the geometrical notation is introduced. For a gradually varying topography the alongchannel flow is in geostrophic balance although the velocity changes in the downstream direction. The flow is hence described by

$$vf = g\frac{\partial \eta}{\partial x} \tag{2}$$

$$u\frac{\partial v}{\partial x} + v\frac{\partial v}{\partial y} + fu = -g\frac{\partial \eta}{\partial y}, \tag{3}$$

$$\frac{\partial}{\partial x}(uD) + \frac{\partial}{\partial y}(vD) = 0. \tag{4}$$

Here u and v are the velocity components in the cross- and downstream direction, f the Coriolis parameter, and g the constant of gravity. (For a 1½-layer system g is replaced by the reduced gravity $g' = g\Delta\rho/\rho$, where $\Delta\rho$ is the density difference between the two layers.) The reference level, $z = 0$, is taken to be the highest elevation of the channel floor and η is the surface elevation above this level. The total depth is given by $D = \eta + h$, where $z = -h$ is the position of the bottom.

From Eqs. (2)–(4) the potential vorticity equation can be derived

$$\frac{f + \partial v/\partial x}{D} = G(\psi), \tag{5}$$

where the streamfunction, ψ, is defined by

$$Du = -\frac{\partial \psi}{\partial y}, \quad Dv = \frac{\partial \psi}{\partial x},$$

$$\psi\left(\frac{-w}{2}\right) = \frac{-Q}{2}, \quad \psi\left(\frac{w}{2}\right) = \frac{Q}{2}.$$

Let the potential vorticity in the upstream reservoir be uniform and given by $G = f/D_\infty$. (Note that D_∞ is not necessarily the reservoir depth.) Equation (5) can then be rewritten as

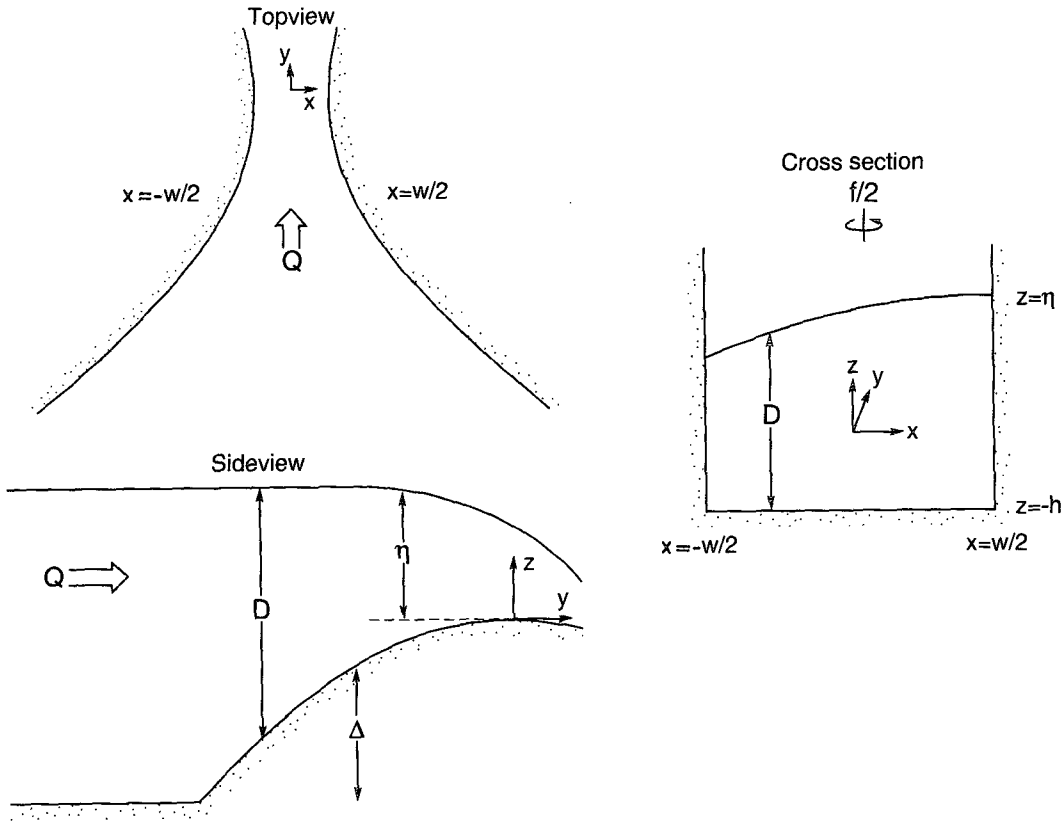

FIG. 1. Definitional sketches of the channel geometry.

$$\frac{\partial v}{\partial x} = f\left(\frac{D}{D_\infty} - 1\right). \tag{6}$$

The potential vorticity and the Bernoulli function are related by $G = dB/d\psi$, and the energy equation is consequently given by

$$\frac{1}{2}v^2 + g\eta = \frac{f\psi}{D_\infty} + C, \tag{7}$$

where C is a constant.

It will now be assumed that in the main portion of a very deep/broad upstream basin, the square of the velocity is negligible compared to $g\eta$. Let $\psi = \psi_i$ be a streamline emanating from this quiescent region. Furthermore, if the velocity shear, $\partial v/\partial x$, in the reservoir is negligible compared to f, then the upstream elevation for this streamline is given by $\eta_\infty = D_\infty - \Delta_{\max}$, where $\Delta_{\max}$ is the maximum height of the sill relative to the bottom floor in the upstream basin. (In later sections, the validity of identifying the potential depth with the depth in the upstream reservoir will be examined.) The constant C can thereby be determined and Eq. (7) becomes

$$\frac{1}{2}v^2 + g\eta = \frac{f}{D_\infty}(\psi - \psi_i) + (D_\infty - \Delta_{\max})g. \tag{8}$$

Equation (8) will be used to compute the along-channel structure of the flow. To find the cross-channel structure, Eqs. (2) and (6) are combined, yielding

$$\frac{\partial^2 \eta}{\partial x^2} - \frac{f^2}{g}\left(\frac{D}{D_\infty} - 1\right) = 0. \tag{9}$$

Since the bottom is flat across the channel, η may be interchanged by D in Eqs. (2) and (9). Before proceeding, the variables are nondimensionalized using the following scales for width, velocity, and depth:

$$w_s = 2(gD_\infty)^{1/2}/f,\ v_s = \left(\frac{fQ}{2D_\infty}\right)^{1/2},\ D_s = \left(\frac{fQ}{2g}\right)^{1/2}.$$

This choice of scaling is consistent with volume conservation ($Q = w_s v_s D_s$) and the geostrophic relation ($fv_s/2 = gD_s/w_s$). (In particular, w_s and D_s are the scale width and depth of a current having volume transport Q and potential depth D_∞, flowing along a single lateral boundary such that D vanishes at the offshore edge.) The nondimensional variables are thus defined as

$$x^* = x/w_s,\quad w^* = w/w_s,\quad D^* = D/D_s,$$

$$v^* = v/v_s,\quad \psi^* = \psi/Q,\quad \Delta^* = \frac{\Delta}{D_\infty}.$$

Using the identity $\eta = D - (\Delta_{\max} - \Delta)$ in the energy equation, the nondimensional form of Eqs. (2), (6), (8), and (9) becomes

$$v = \frac{1}{2}\frac{\partial D}{\partial x} \tag{10}$$

$$\frac{1}{2}\frac{\partial v}{\partial x} = \hat{D}_\infty\left(\frac{D}{\hat{D}_\infty} - 1\right), \tag{11}$$

$$\frac{1}{2\hat{D}_\infty}v^2 + D = \frac{2}{\hat{D}_\infty}(\psi - \psi_i) + \hat{D}_\infty(1 - \Delta), \tag{12}$$

$$\frac{\partial^2 D}{\partial x^2} - 4\hat{D}_\infty\left(\frac{D}{\hat{D}_\infty} - 1\right) = 0. \tag{13}$$

(Here the stars, indicating the nondimensional variables, have been dropped.) The parameter $\hat{D}_\infty$ in Eqs. (10)–(13) is defined by

$$\hat{D}_\infty = \frac{D_\infty}{D_s} = \left(\frac{2D_\infty^2 g}{fQ}\right)^{1/2},$$

the ratio of the potential depth to the scale depth D_s. This quantity is the nondimensional measure of the potential vorticity. The scale depth is determined by f, g, and Q; and Q is regulated by the sill height $\Delta_{\max}$ or minimum width under conditions of critical control. Thus, the nondimensional measure of the magnitude of potential vorticity varies with the geometry of the controlling topography, even when the upstream value of D_∞ is held constant.

The solution to differential equation (13) is given by

$$D = \hat{D}_\infty + \hat{D}_\infty\left(\frac{\bar{D}}{\hat{D}_\infty} - 1\right)\frac{\cosh 2x}{\cosh w} + \delta D\frac{\sinh 2x}{\sinh w}, \tag{14}$$

where

$$\bar{D} = \frac{1}{2}\left[D\left(\frac{w}{2}\right) + D\left(-\frac{w}{2}\right)\right];$$

$$\delta D = \frac{1}{2}\left[D\left(\frac{w}{2}\right) - D\left(-\frac{w}{2}\right)\right].$$

The expression for the velocity immediately follows from Eq. (10):

$$v = \hat{D}_\infty\left(\frac{\bar{D}}{\hat{D}_\infty} - 1\right)\frac{\sinh 2x}{\cosh w} + \delta D\frac{\cosh 2x}{\sinh w}. \tag{15}$$

When $w \gg 1$, the channel width is much greater than the Rossby radius of deformation based on D_∞. In this limit the flow takes on a boundary-layer structure, with v proportional to $\exp(\pm 2x - w)$ as $x \to \pm -w$.

The Bernoulli equation is now applied on the two boundary streamlines in order to determine $\bar{D}$ and δD. This yields an algebraic equation for $\bar{D}$

$$4\psi_i + t^2\hat{D}_\infty^2\left(\frac{\bar{D}}{\hat{D}_\infty} - 1\right)^2 + \frac{1}{t^2\bar{D}^2} + 2\hat{D}_\infty^2\left(\frac{\bar{D}}{\hat{D}_\infty} - 1 + \Delta\right) = 0, \tag{16}$$

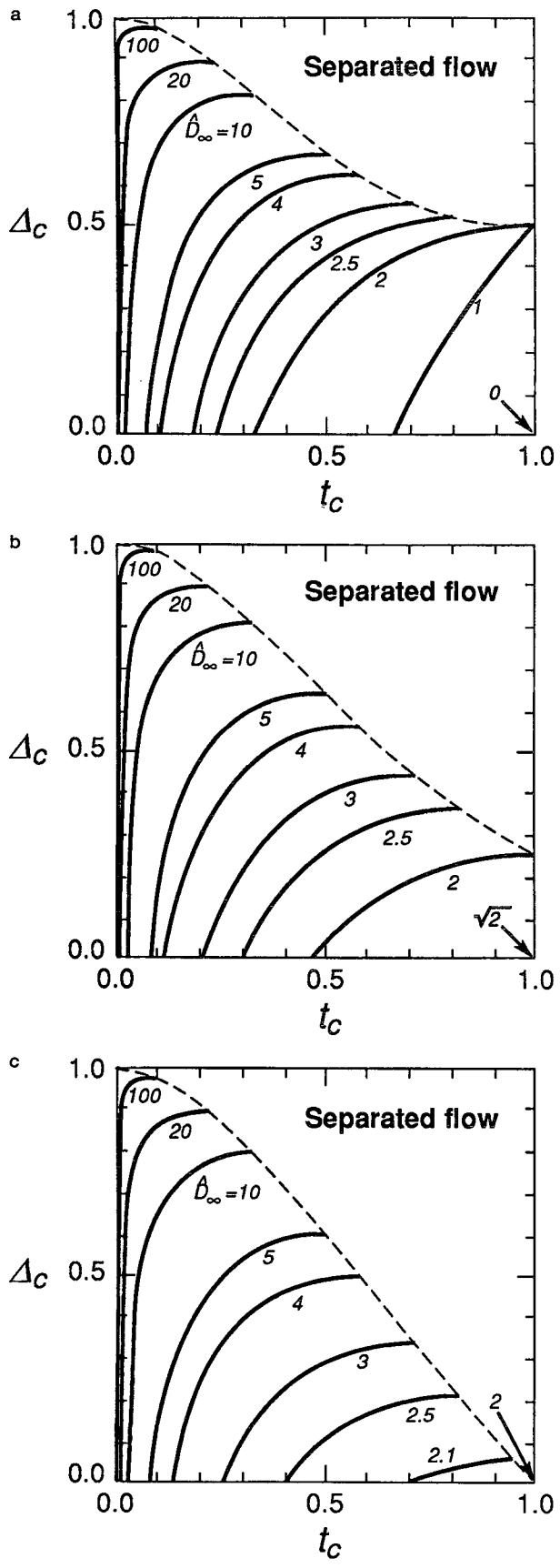

where $t = \tanh(w)$. After $\bar{D}$ has been computed, δD is given by

$$\delta D \bar{D} = 1. \tag{17}$$

Equations (16) and (17) are the same as those presented by Gill (1977), with the exception that here the topographic parameter Δ has been scaled with D_∞ instead of D_s.

The solutions to Eq. (16) will be discussed in more detail in sections 5 and 6, but some general features will be outlined here. For each set of $\hat{D}_\infty$, ψ_i, w, and Δ at most two solutions exist for a flow in the positive y direction. As the geometry varies, the two branches, representing a sub- and supercritical flow, respectively, may merge into a branch point beyond which no solution exists for the particular parameters chosen. The branch point solution is critical, or controlled, since no downstream disturbances can travel through the constriction and alter the upstream conditions. This solution can only exist at a geometrical extremum of the channel. The controlled flow is of particular importance since it represents the largest possible transport through the channel for the given upstream conditions.

The examples discussed in the following sections are restricted to unidirectional upstream flows, that is, flows for which $-1/2 \leq \psi_i \leq 1/2$. The case $\psi_i = 0$ corresponds to an upstream flow equally divided between the two boundary layers. For $\psi_i = -1/2$, the flow is confined to the right-hand boundary (looking in the downstream direction), whereas for $\psi_i = 1/2$ the flow is along the left-hand wall. Only geometries for which the fluid wets the floor all across the channel will be considered. When the flow becomes separated, the depth on the left-hand side equals zero, and from (17) and the definitions of $\bar{D}$ and δD, it follows that $\bar{D} = 1$.

To illustrate the numerous combinations of critical width/critical sill height for a given value of the parameter $\hat{D}_\infty$, Figs. 2a–c have been constructed for $\psi_i = -1/2$, 0, and $1/2$. (The dashed line indicates the demarcation between separated and nonseparated flow at the critical section.)

3. The problem of identifying the "potential" depth

To apply the hydraulic theory for constant potential vorticity, it is necessary to know the potential depth D_∞. In practical applications it is natural to identify D_∞ with the upstream depth at some interior location. The key requirement is that the choice be consistent with the results generated by the hydraulic theory using

FIG. 2. Controlled solutions for a flow of constant (but nonzero) potential vorticity given as critical width [$tc = \tanh(w_c)$] versus critical sill height for various $\hat{D}_\infty$. Above the dashed line the flow has separated at the control section: (a) $\psi_i = -1/2$, (b) $\psi_i = 0$, (c) $\psi_i = 1/2$.

this specific value of D_∞. The choice is consistent with the theory if the assumptions made in the Bernoulli equation are satisfied; that is, the kinetic energy must be negligible compared to the potential energy in the interior upstream basin and the relative vorticity must be negligible compared to f. The first requirement may be expressed as $v^2[2g\eta_\infty]^{-1} \ll 1$ and the second as $(\partial v/\partial x)f^{-1} \ll 1$ or equally $D/D_\infty \approx 1$ [see Eq. (1)].

In this section, an attempt will be made to determine the minimum upstream width and/or depth required to make the choice of D_∞ compatible with the assumptions made in the Bernoulli equation. Put differently, does the hydraulic theory predict an interior depth that is close to the one observed (the depth which is taken to represent D_∞) in a particular upstream basin? Is the velocity predicted by the theory small enough there? To answer these questions, the solutions are followed upstream from the control section and the depth and velocity profiles are calculated for the midchannel (between $x = -w/4$ and $x = w/4$). If the kinetic energy is less than 5% of the potential energy over the interval $[-w/4, w/4]$ and if also the difference between the depth and D_∞ is less than 5% over the same interval, then the chosen value of D_∞ is taken to be acceptable.

Since the combinations of different upstream configurations are infinite for a given width of the control section, the investigation is limited to four basic channel geometries. The first is a channel of constant depth that widens upstream, and in Figs. 3a–c the results are presented. For any width (t_c) of the control section the graphs indicate the minimum width of the upstream basin required to let the assumed potential depth be identified as the upstream interior depth. In the main graphs the delimiting curves are shown in the $t_c - t$ space. For clarity, when t_c is close to 1 the diagrams are presented in the $w_c - w$ space.

The figures show that, as a general rule, the upstream width has to be at least two times the Rossby radius of deformation ($t \geq 0.96$) unless the channel is very narrow at the control section ($t_c \leq 0.1$). It is also demonstrated that for flows characterized by $\psi_i = 0$ and $\psi_i = 1/2$, the requirements above are satisfied already at the control if this section is very wide ($w_c \approx 6$). It is a bit different for $\psi_i = -1/2$, that is, when the upstream flow is confined to the right-hand wall. The parameter $\hat{D}_\infty$ now has to be very small for controlled solutions to exist if the critical width, w_c, is larger than about 2 (see Fig. 2a). The upstream depth profile displays a very shallow layer in the interior and left part of the basin, while the surface rises to $D \approx 2$ toward the right-hand wall. Although the absolute difference between the interior and the potential depth is as small as in the case of $\psi_i = 1/2$, the relative difference is much larger. Therefore, the upstream basin now has to be very wide for the assumed potential depth to be identified as the interior upstream depth.

In Fig. 4, a graph similar to Fig. 3 has been constructed for the case of a channel that deepens upstream. The depth and velocity profiles have been calculated in the upstream basin, where $\Delta = 0$, for all combinations of critical widths and sill heights for which the flow remains attached to the walls at the control section. The upstream width has been taken to be equal to the critical width w_c (solid curve), two times w_c (dashed curve), and four times w_c (dotted curve). The thin dashed curve indicates separation at the control section.

For the first configuration, ($w_{\text{upstream}} = w_c$) sill heights between 0.4 and 0.7 are required for the assumed potential depth to be identified as the upstream interior depth. The lower values of the sill height pertain to narrow channels, and for these widths ($t < 0.1$) there is no significant difference between flows with different values of the parameter ψ_i. There is, however, a second regime for which the assumed potential depth may be identified as the upstream interior depth and that is for t_c close to 1. For $\psi_i = 0$ this regime starts at $w_c \approx 3.5$ and $\Delta \approx 0.25$, and when w_c is increased the required height of the sill decreases down to zero as pictured in Fig. 4b. Here the critical width is around 6 (see also Fig. 3b). For $\psi_i = 1/2$, the height of the sill is very close to zero for nonseparated solutions to exist. (This regime is indicated by the dot in the lower right corner in Fig. 4c.) Hence, the critical width has to be close to, or larger than, ~6, as was shown in Fig. 3c. Finally, for $\psi_i = -1/2$ this second regime starts at $w_c \approx 4.2$ and $\Delta \approx 0.5$ (indicated by the dot in Fig. 4a). The flow is very close to separation and the picture remains the same for critical widths up to around 10. For larger values the accuracy in the calculations becomes unsatisfactory.

For $w_{\text{upstream}} = 2w_c$ the required sill height is reduced to zero for channels with very narrow control sections. Also, for any critical width the required sill height is generally reduced by increasing the upstream width. The second regime starts, for $\psi_i = -1/2$, at $w_c \approx 2.1$ and $\Delta_c \approx 0.5$. The required height remains the same for critical widths up to around 10, after which no calculations were made. For $\psi_i = 0$, the second regime starts at $w_c \approx 1.5$ and $\Delta_c \approx 0.3$, and the minimum sill height is reduced to zero when the critical width is larger than 2.85. When $\psi_i = 1/2$, the critical width has to be larger than 2.9 in the wide channel regime where, again, the sill height is very close to zero.

For the third configuration, $w_{\text{upstream}} = 4w_c$, a further reduction of the required sill height is demonstrated. For channels with narrow control sections the minimum sill height is zero and the same is true when $w_c \geq 1.35$ ($\psi_i = 0$) and $w_c \geq 1.75$ ($\psi_i = 1/2$). In the case of $\psi_i = -1/2$ the minimum sill height for wide control sections is $\Delta_c \approx 0.4$. Again, no calculations were made for $w_c > 10$.

A specific example will now be given to demonstrate the use of the figures in this section. Consider the case of a sill overflow that is believed to be maximized and suppose that hydraulic theory will be used to estimate

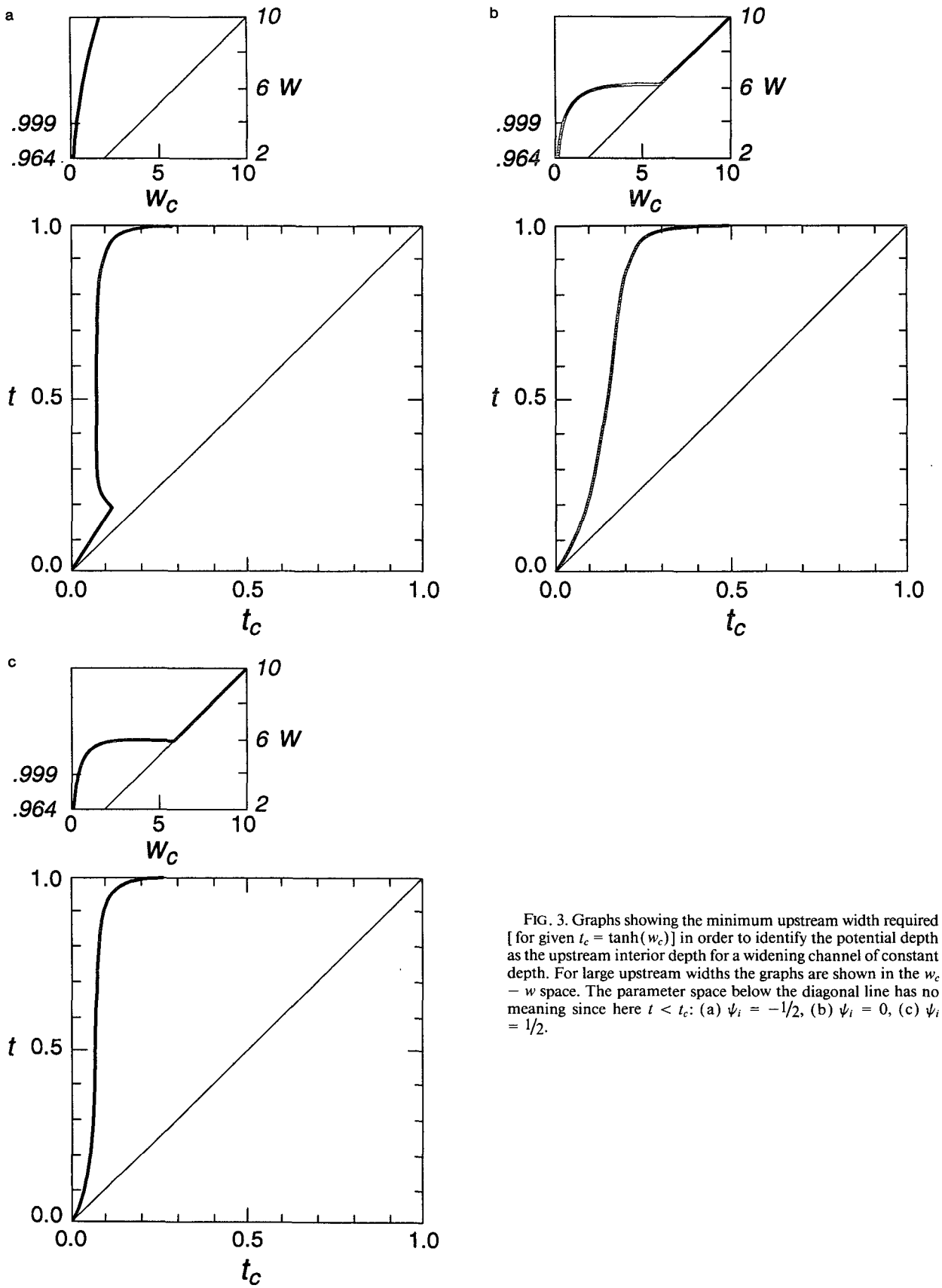

FIG. 3. Graphs showing the minimum upstream width required [for given $t_c = \tanh(w_c)$] in order to identify the potential depth as the upstream interior depth for a widening channel of constant depth. For large upstream widths the graphs are shown in the $w_c - w$ space. The parameter space below the diagonal line has no meaning since here $t < t_c$: (a) $\psi_i = -1/2$, (b) $\psi_i = 0$, (c) $\psi_i = 1/2$.

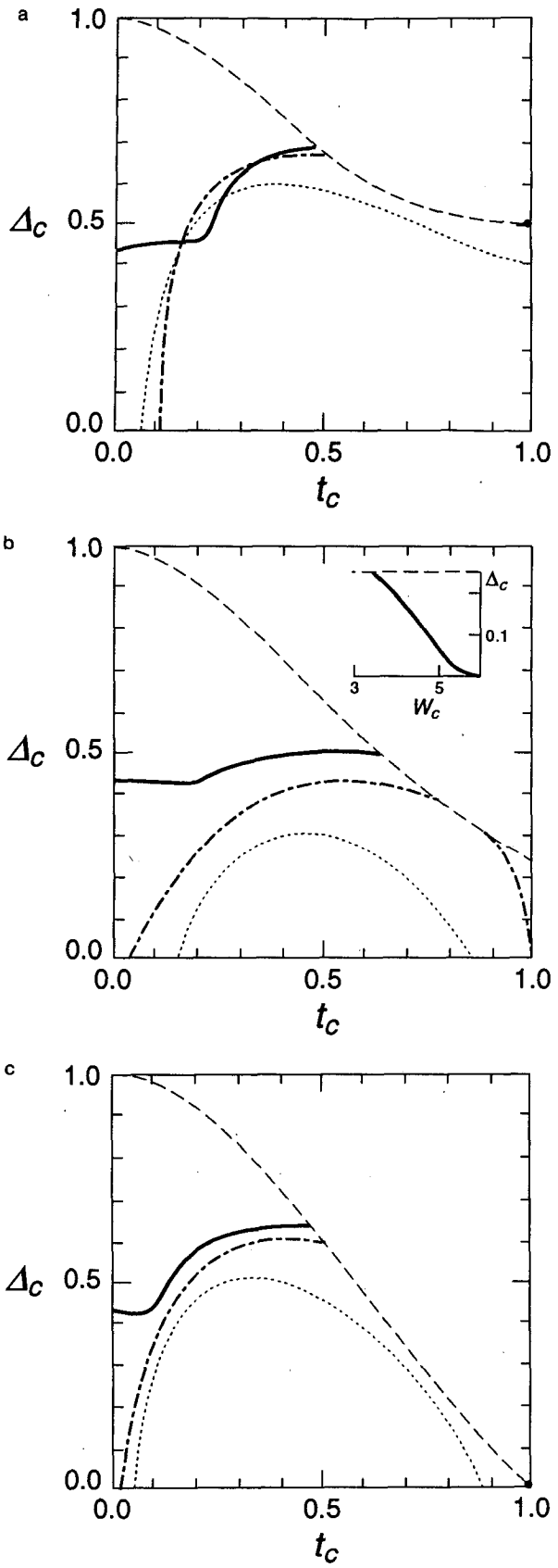

the transport. Suppose also that a hydrographic cross section has been taken at a location in the upstream basin where the width has increased to twice the width at the sill. At this section the interface is flat in the interior, and the depth below the interface is therefore chosen to represent the potential depth, D_∞. Assume that the sill width is 10 km, the interior depth 1000 m, the reduced gravity 10^{-3} m^2 s^{-1}, the Coriolis parameter 10^{-4} s^{-1}, and the sill height (measured as the height of the sill crest above the bottom where the upstream section was taken) 350 m. The nondimensional values of the critical width and sill height become $w_c = 0.5$ ($t_c \approx 0.46$) and $\Delta_c = 0.35$, respectively. When entering these values of t_c and Δ_c in Fig. 4, one concludes that regardless of the upstream distribution of the flow (i.e., ψ_i), the assumed value of D_∞ is not compatible with the theory since the point $t_c \approx 0.46$, $\Delta_c = 0.35$ lies below the dashed curve in all the three panels. (The upstream width was twice the critical width and therefore the dashed curves should be used.) According to the hydraulic theory, the interior depth at an upstream cross section that is twice the critical width should differ from D_∞ by more than 5%. Hence, the observed flow field is in this case incompatible with the theory. This situation could occur if, for example, the observed flow is not controlled, the potential vorticity is not uniform, the velocities in the interior of the upstream basin are not close to zero, or the friction is not negligible. Had the upstream cross section been wider, say four times the width at the control section, the assumed value of D_∞ would have been consistent with the hydraulic theory, provided that the upstream flow distribution was characterized by $\psi_i = 0$.

4. The deep reservoir–narrow channel limit

The deep reservoir–narrow channel limit is obtained by assuming that the right-hand side of Eq. (1), f/D_∞, is much smaller than both f/D and $D^{-1}(\partial v/\partial x)$. These assumptions imply that the fluid depth is much less than the potential depth ($D \ll D_\infty$) and that the width of the channel is much less than the Rossby radius of deformation based on the potential depth ($w^2 \ll gD_\infty/f^2$). The vorticity equation (11) now becomes $\partial v/\partial x \approx -2\hat{D}_\infty$, which in dimensional form is $\partial v/\partial x \approx -f$. In the Bernoulli equation (12) the term $2(\psi - \psi_i)/\hat{D}_\infty$ will be much smaller than any of the other terms

FIG. 4. Graphs showing the minimum sill height required [for given $t_c = \tanh(w_c)$] in order to identify the potential depth as the upstream interior depth for a channel that deepens upstream. The solid curve pertains to a channel of constant width. The dashed curve shows the results for a channel with an upstream width equal to $2w_c$. For the dotted curve the upstream width equals 4 w_c. The dots in panels a and c show the minimum sill height in the limit $t_c \to 1$. (See text for details.) Above the thin dashed line the flow has separated at the control section: (a) $\psi_i = -1/2$, (b) $\psi_i = 0$, (c) $\psi_i = 1/2$.

and may hence be neglected. The differential equation (13) is reduced to

$$\frac{\partial^2 D}{\partial x^2} + 4\hat{D}_\infty = 0, \tag{18}$$

with the solution

$$D = \bar{D} - \hat{D}_\infty\left(2x^2 - \frac{w^2}{2}\right) + \frac{2\delta D x}{w}. \tag{19}$$

From Eq. (10) it follows that the corresponding velocity becomes

$$v = -2\hat{D}_\infty x + \frac{\delta D}{w}. \tag{20}$$

To determine $\bar{D}$ and δD the continuity equation together with Bernoulli equation (applied along one of the boundary streamlines) are used. The resulting equation for $\bar{D}$ is

$$w^2\hat{D}_\infty^2 + \frac{1}{w^2\bar{D}^2} + 2\hat{D}_\infty^2\left(\frac{\bar{D}}{\hat{D}_\infty} - 1 + \Delta\right) = 0, \tag{21}$$

and again the relationship between $\bar{D}$ and δD is given by Eq. (17). [Note that Eq. (21) can be derived directly from Eq. (16) if the term involving ψ_i is ignored and the approximations $\tanh(w) \approx w$ and $\bar{D}/\hat{D}_\infty \ll 1$ are made. Within the parentheses in Eq. (21) the term $\bar{D}/\hat{D}_\infty$ has to be kept since $\Delta - 1$ might also be small.] These expressions for D, v, and $\bar{D}$ are those associated with the so-called zero potential vorticity approximation.

Equation (21) is a third-order equation in $\bar{D}$ and the roots are given by

$$\bar{D}_i = \frac{\hat{D}_\infty}{3}\left[1 - \Delta - \frac{w^2}{2}\right][1 - 2\cos\Theta_i], \tag{22}$$

where

$$\Theta_1 = \Theta, \quad \Theta_2 = \Theta + \frac{2\pi}{3}, \quad \Theta_3 = \Theta + \frac{4\pi}{3},$$

and Θ is obtained from

$$\cos 3\Theta = \left(\frac{27}{4\hat{D}_\infty^4 w^2(1 - \Delta - w^2/2)^3} - 1\right).$$

Only two of the solutions correspond to a physically realizable flow. The branch point at which the two solutions coalesce is characterized by $\cos 3\Theta = 1$ or $8\hat{D}_\infty^4 w_c^2(1 - \Delta_c - w_c^2/2)^3/27 = 1$. Here the transport is maximized for a given geometry and potential depth. In dimensional form the maximum transport becomes

$$Q = \left(\frac{2}{3}\right)^{3/2} w_c g^{1/2}\left[(D_\infty - \Delta_c) - \frac{w_c^2 f^2}{8g}\right]^{3/2}.$$

This is exactly the expression presented by Whitehead et al. (1974). The upstream elevation above the sill, corresponding to h_u in Whitehead et al. (1974), is represented here by $D_\infty - \Delta$.

It is only for the deep reservoir–narrow channel limit that simple, explicit solutions exist. Hence, it is desirable to try to establish the parameter range for which these solutions give an accurate description of a constant (nonzero) potential vorticity flow.

All possible controlled solutions for a constant (nonzero) potential vorticity flow (that is unidirectional in the upstream basin) have already been presented in Figs. 2a–c. The corresponding graph for the simplified flow [based on Eq. (21)] is shown in Fig. 5. To facilitate a comparison between the constant potential vorticity model and the simplified model, the graphs for the former have been overlaid in Fig. 5 using dashed curves.

The first thing to notice when comparing the controlled solutions is that for $t_c < 0.1$, there is hardly any difference between the two models. It might seem surprising that the solutions agree so well even when the sill height is very low (and the approximation $\bar{D}/\hat{D}_\infty \ll 1$ is very poor). The reason can be found after examining the second term in Eq. (16) and the first in Eq. (21). These terms are proportional to the difference between the squares of the velocities on either wall at the control section. If the channel is very narrow and the sill low, the velocity difference across it will be small. Therefore the second term in Eq. (16) and the first in Eq. (21) is almost negligible for these geometries and, since $\tanh(w) \approx w$ is a very good approximation for small w and the importance of ψ_i quickly diminishes as $\hat{D}_\infty$ is increased, the two equations become nearly identical.

Another feature demonstrated in Fig. 5 is that the controlled flow described by the simplified equations generally separates for lower values of the critical sill and width (for given $\hat{D}_\infty$) compared to the constant (nonzero) potential vorticity flow. Only for narrow channels with large sill heights will separation occur for the same geometry. The former flow will separate when $w_c^2 > (1 - \Delta_c)/2$. Transforming this expression to dimensional form gives the same criterion as the one given by Whitehead et al. (1974). A flow of constant (nonzero) potential vorticity separates when

$$t_c^2 > \frac{-\Delta_c}{2\psi_i + \Delta_c} + \left[\frac{2\psi_i + \Delta_c - 2\psi_i\Delta_c}{(2\psi_i + \Delta_c)^2}\right]^{1/2}.$$

As mentioned in section 2, the controlled solution represents the maximum flow rate for a given geometry and potential depth. To compare the accuracy of the flow rates predicted by the simplified model, Fig. 6 has been constructed. In the graph the ratio of the maximum transport for a deep reservoir–narrow channel flow to the maximum transport obtained for a constant (nonzero) potential vorticity flow has been computed for a given potential depth and geometry at the control section. Again it is demonstrated that for narrow chan-

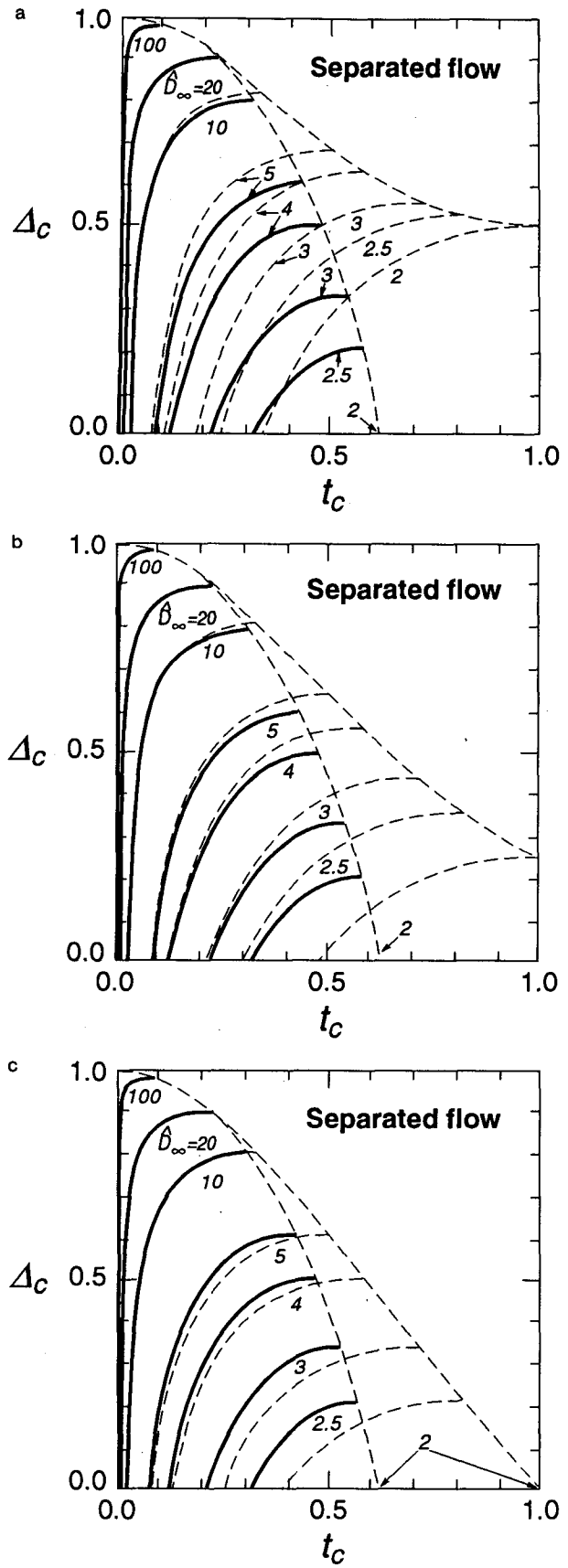

nels the agreement is very good for all three upstream flow figurations. In particular, for flows characterized by $\psi_i = 0$ and $\psi_i = 1/2$, the transports given by the simplified model will never differ with more than around 20% regardless of the geometry at the control section (provided that the flow has not separated). Whitehead (1989) compared the flow obtained from the simplified model and a constant potential vorticity flow (corresponding to the case $\psi_i = 1/2$) for a widening channel of constant depth ($\Delta_c = 0$). He found that the difference in maximum flow rate was at most around 20%. As Fig. 6b indicates, this number decreases when a sill is introduced.

When comparing the simplified solutions with those of a constant (nonzero) potential vorticity flow for which $\psi_i = -1/2$, the agreement rapidly diverges when t_c is increased. The approximation underestimates the maximum flow rate by up to two-thirds for the worst possible case. Another feature demonstrated in Fig. 6 is that the width affects the results much more than the sill height, especially when $\psi_i = -1/2$ or 0.

A somewhat surprising behavior is shown in Fig. 6c for the case $\psi_i = 1/2$. Here the agreement first decreases as the width of the control section is increased, as expected. However, at some point the solutions get closer together as the width increases and the improvement continues until the zero potential vorticity flow separates. When the upstream flow is confined to the left-hand wall, the initial velocity shear and its redistribution at the control section is such that for a given geometry and potential depth, a smaller amount of water is carried through the channel compared to, for example, the case when $\psi_i = -1/2$ (see Fig. 2). If the width at the control section is increased (for fixed Δ and dimensional potential depth) the increase in transport (or equally the decrease in $\hat{D}_\infty$) is smaller for $\psi_i = 1/2$ than for $\psi_i = -1/2$. At the same time the decrease of the mean depth, $\bar{D}$, is larger for $\psi_i = 1/2$ than for $\psi_i = -1/2$. The result is that when $\psi_i = -1/2$, the ratio $\bar{D}/\hat{D}_\infty$ grows as the critical width is increased, while for $\psi_i = 1/2$ this ratio actually decreases. Hence, for the latter flow the assumption that $\bar{D}/\hat{D}_\infty \ll 1$ becomes more accurate as the width of the control section increases as opposed to the assumption that $\tanh(w_c) \approx w_c$. The features shown in Fig. 6c could therefore be explained by the combined effect of the two approximations used in the second term in Eq. (21).

5. A channel of constant depth that widens upstream

In this section, the case of a channel of constant depth that widens upstream will be examined in more

FIG. 5. Controlled solutions obtained from the narrow channel–deep reservoir approximation given as critical width [$t_c = \tanh(w_c)$] versus critical sill height for various $\hat{D}_\infty$. The solutions are superimposed on those of a constant (nonzero) potential vorticity flow presented in Figs. 2a–c (shown here as thin dashed curves): (a) $\psi_i = -1/2$, (b) $\psi_i = 0$, (c) $\psi_i = 1/2$.

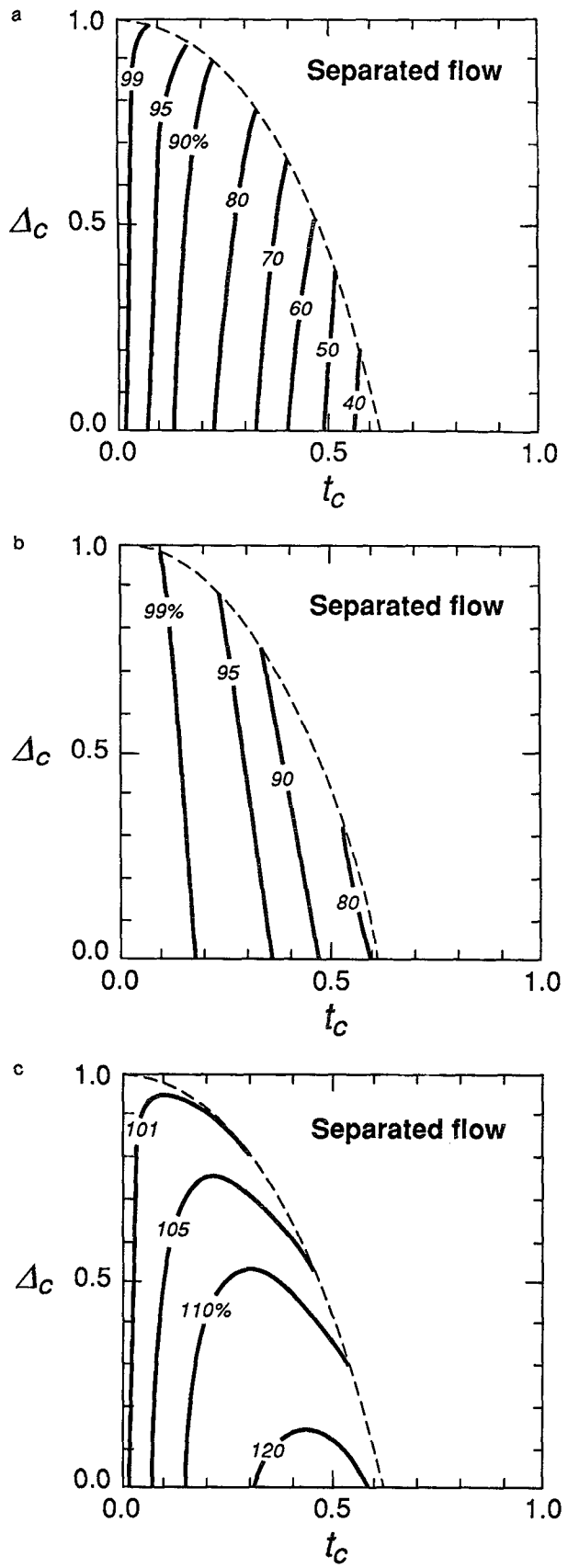

detail. For this geometry the constant (nonzero) potential vorticity flow is described by Eqs. (14)–(16), where Δ is put equal to zero. The solutions of Eq. (16) for $\psi_i = -1/2, 0, 1/2$ are shown as solid curves in Figs. 7a–c. Each curve relates the average wall depth $\bar{D}$ to the width of the channel for given potential depth $\hat{D}_\infty$. The thin solid line in each graph indicates the branch point, or the controlled, solutions. This curve corresponds to the x axis in Figs. 2a–c. (Other horizontal cuts for which the depth remains constant when moving upstream will show the same pattern, since it is only a question of changing the origin of the z axis.) Above the thin curve the flow is subcritical, whereas it is supercritical below it. For $\bar{D} \leq 1$, the flow is separated from the left-hand wall, looking in the downstream direction.

The problem discussed now is how far upstream the deep reservoir–narrow channel approximation can be used. The simplified solutions obtained from Eq. (21) are shown as dashed curves in Figs. 7a–c. (Since these solutions are independent of ψ_i, the dashed curves are identical in the three graphs.) The critical widths are taken to be the same as for the constant (nonzero) potential vorticity flow. To obtain controlled solutions for these widths, the values of $\hat{D}_\infty$ have to be modified for the simplified flow, as indicated in the graphs. The branch point solution for the approximation is given by the thin dashed line.

For the flat bottom geometry there is no section in the channel where the inequality $\bar{D}/\hat{D}_\infty \ll 1$ holds. But, as was pointed out in the previous section, as long as the width of the channel is very small, the term representing the cross-stream variation of the velocity [i.e., the second term in Eq. (16) and the first term in Eq. (21)] will be negligible. Consequently there is a good agreement between the solution curves for small values of t. Even for somewhat larger widths, the controlled solutions for $\bar{D}$ show a good agreement. When comparing the solutions of Eqs. (16) and (21), it turns out that deviations of the latter from the former will appear in the depth profile rather than in the mean depth.

Following the solutions upstream from the critical section, the branch corresponding to a subcritical flow obtained from the simplified equations (the upper part of the dashed solution curves) soon diverges from the curve describing a subcritical flow of constant (nonzero) potential vorticity flow. Eventually the former will separate from the left-hand wall and, as the channel widens, an increasing part of the floor will become dry.

FIG. 6. The ratio of the maximum transport obtained from the simplified model to the maximum transport for a constant (nonzero) potential vorticity flow for given potential depth and geometry at the control section. Above the dashed line the former flow has separated at the control section: (a) $\psi_i = -1/2$, (b) $\psi_i = 0$, (c) $\psi_i = 1/2$.

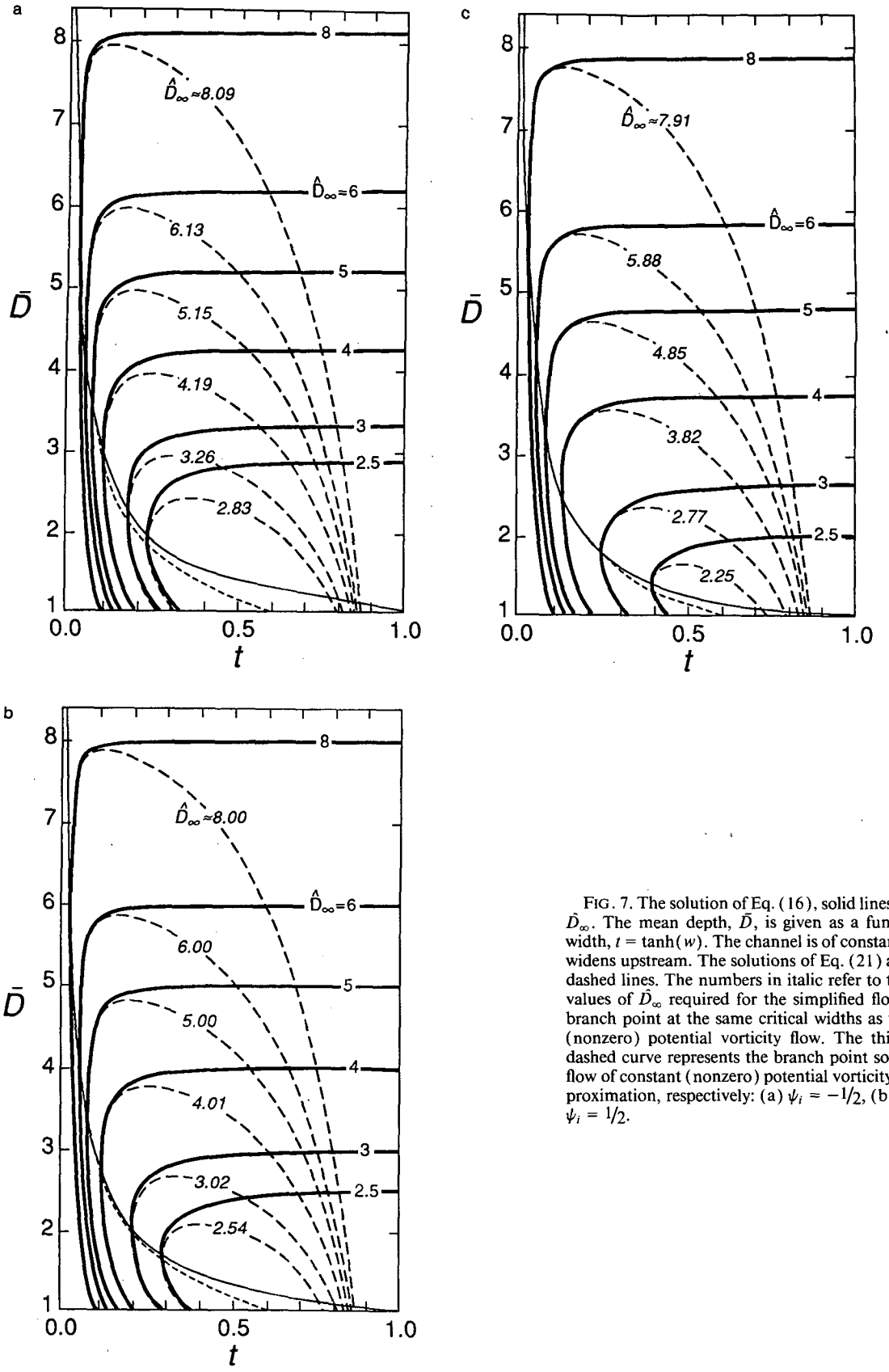

FIG. 7. The solution of Eq. (16), solid lines, for various $\hat{D}_\infty$. The mean depth, $\bar{D}$, is given as a function of the width, $t = \tanh(w)$. The channel is of constant depth and widens upstream. The solutions of Eq. (21) are shown as dashed lines. The numbers in italic refer to the modified values of $\hat{D}_\infty$ required for the simplified flow to have a branch point at the same critical widths as the constant (nonzero) potential vorticity flow. The thin solid and dashed curve represents the branch point solutions for a flow of constant (nonzero) potential vorticity and the approximation, respectively: (a) $\psi_i = -1/2$, (b) $\psi_i = 0$, (c) $\psi_i = 1/2$.

Despite the fact that there is a streamline in the upstream basin on which $v = 0$, this flow configuration does not in any way resemble the kind of upstream scenario outlined in section 2.

The results discussed above will now be illustrated by an example that describes a controlled flow through a narrow channel ($t_c = 0.08$). For the constant (nonzero) potential vorticity flow ψ_i is chosen to be 1/2, and Fig. 7c shows that the maximum flow for this geometry is obtained for $\hat{D}_\infty = 5$. The corresponding value of $\hat{D}_\infty$ for the simplified model is around 4.85. The difference in maximum transport in this case is close to 6%. In Figs. 8a and 8b, the velocity distribution is shown for the two models, starting at the control section and going upstream to a width $w \approx 7w_c$. The depth profiles are also given (in Fig. 8c) at the control section and at sections where the channel has widened to 2.5 and 7 times, respectively, the width at the narrow. The deep reservoir–narrow channel approximation is very accurate at the control section. When $w \approx 2.5w_c$ (section B) the depth structures agree fairly well but the difference in slope is large enough for the velocity profiles to diverge. For the upstream situation ($w \approx 7w_c$, section C) there is no similarity between the constant (nonzero) potential vorticity flow and the approximation. The latter flow exhibits a large recirculation area and high velocities, whereas the former shows the preassumed conditions of a quiescent upper basin. The recirculation is in consequence of the fixed velocity shear ($-2\hat{D}_\infty$), which characterizes the simplified flow. The wider the channel gets, the larger the required velocity difference between the two channel walls.

6. A channel of constant width that deepens upstream

The solutions of Eqs. (16) and (21) will now be compared for channels of constant width that deepen upstream. The results presented are for a channel/basin of width $t = 0.3$ and $t = 0.5$, respectively. Equation (16) has been solved for various values of $\hat{D}_\infty$, for which different critical sill heights are obtained. When calculating the corresponding solutions for the deep reservoir–narrow channel flow, the values of $\hat{D}_\infty$ have to be modified when inserted in expression (22) in order to get a critical flow for the same channel geometries.

In Figs. 9a–c, the results are shown for a channel/basin of $t = 0.3$ and $\psi_i = -1/2$, 0, and 1/2. [As before,

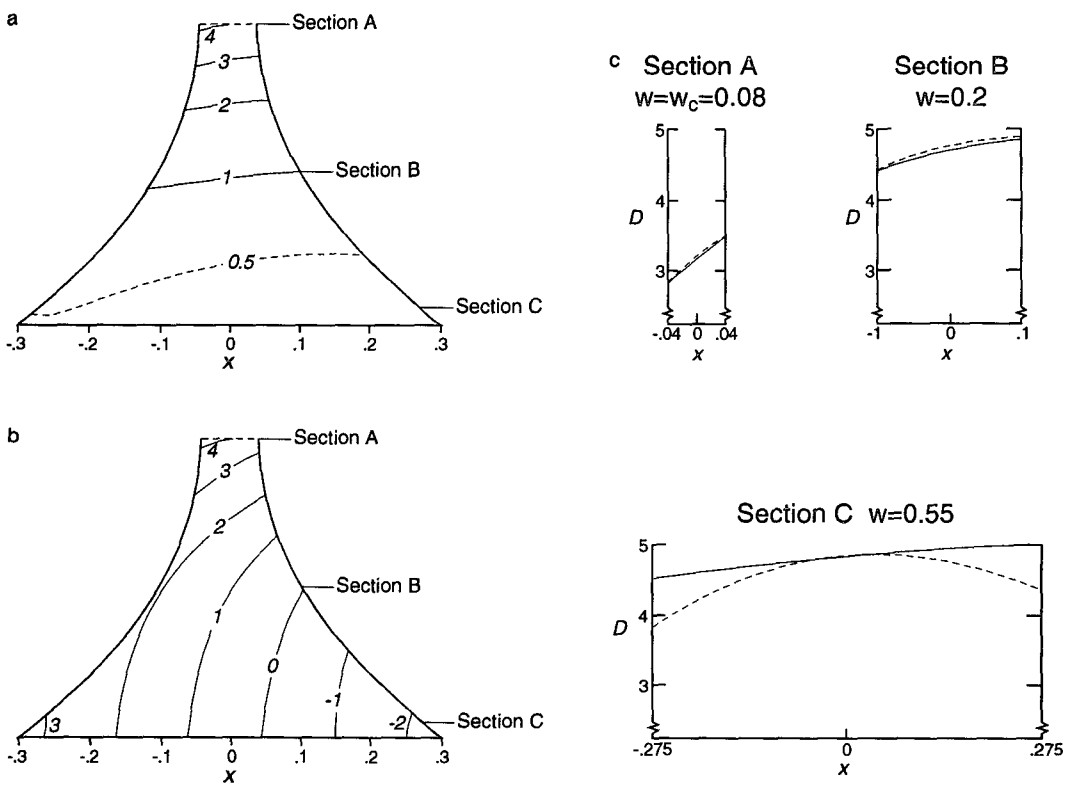

FIG. 8. (a) Velocity field for a controlled flow of constant (but nonzero) potential vorticity in a channel of constant depth that widens upstream. The critical width is given by $t_c = \tanh(w_c) = 0.08$. The flow is characterized by $\hat{D}_\infty = 5$ and $\psi_i = 1/2$. (b) Velocity field for a controlled flow described by the narrow channel–deep reservoir model. The channel geometry is the same as in (a), and $\hat{D} \approx 4.85$. (c) Depth profiles at the control section $t_c = 0.08$ ($w_c \approx 0.08$), for $t = 0.2$ ($w \approx 0.2$) and $t = 0.5$ ($w \approx 0.55$). Solid lines pertain to the constant (nonzero) potential vorticity flow and dashed lines to the simplified flow.

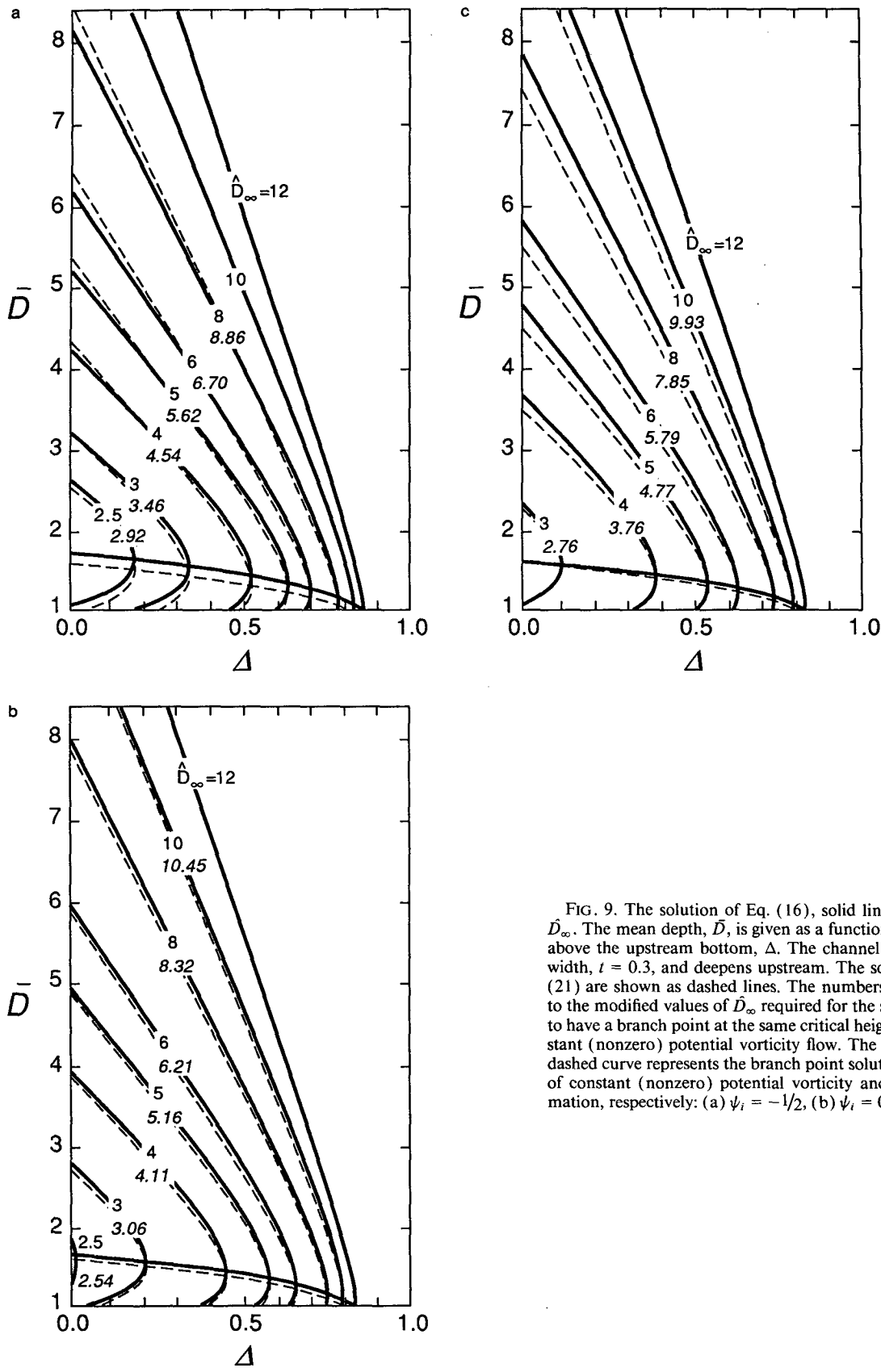

FIG. 9. The solution of Eq. (16), solid lines, for various $\hat{D}_\infty$. The mean depth, $\bar{D}$, is given as a function of the height above the upstream bottom, Δ. The channel is of constant width, $t = 0.3$, and deepens upstream. The solutions of Eq. (21) are shown as dashed lines. The numbers in italic refer to the modified values of $\hat{D}_\infty$ required for the simplified flow to have a branch point at the same critical heights as the constant (nonzero) potential vorticity flow. The thin solid and dashed curve represents the branch point solutions for a flow of constant (nonzero) potential vorticity and the approximation, respectively: (a) $\psi_i = -1/2$, (b) $\psi_i = 0$, (c) $\psi_i = 1/2$.

the solution of Eq. (21) is independent of ψ_i; therefore, the curves for the zero potential vorticity flow are the same in the three graphs.] The channel width is somewhat larger in Fig. 10, $t = 0.5$. The thin solid and thin dashed curves represent the maximum flow solutions, corresponding to vertical cuts in Figs. 2 and 5. In contrast to the case of a widening channel, the simplified solution and the constant (nonzero) potential vorticity solution now follow more closely when traced upstream of the sill. However, as t increases the agreement becomes less good and the range of sill heights for which the simplified flow is nonseparated is rapidly reduced relative to the case of a constant (nonzero) potential vorticity flow.

Now, let us take a closer look at a particular channel configuration. The critical width is given by $t_c = 0.3$ and the sill height by $\Delta_c = 0.8$. For the constant (nonzero) potential vorticity flow the value of ψ_i is again taken to be 1/2, and the maximum flow is obtained for $\hat{D}_\infty = 10$ (see Fig. 9c). The corresponding value for the approximation is $\hat{D}_\infty \approx 9.93$, and the difference in transport is only about 1%. Figures 11a,b show the two velocity fields and in Fig. 11c the depth profiles above Δ_c (i.e., η) are given for the control section and for sections where $\Delta = 0.5$ and 0. At the critical section the depth profiles correspond well but the deviation in curvature near the left-hand wall is large enough for the velocity profiles to differ here. For both flows there is a large recirculation area on the upstream side of the sill. When the potential vorticity is constant (but nonzero) the flow becomes unidirectional when the channel flattens out, whereas the deep reservoir–narrow

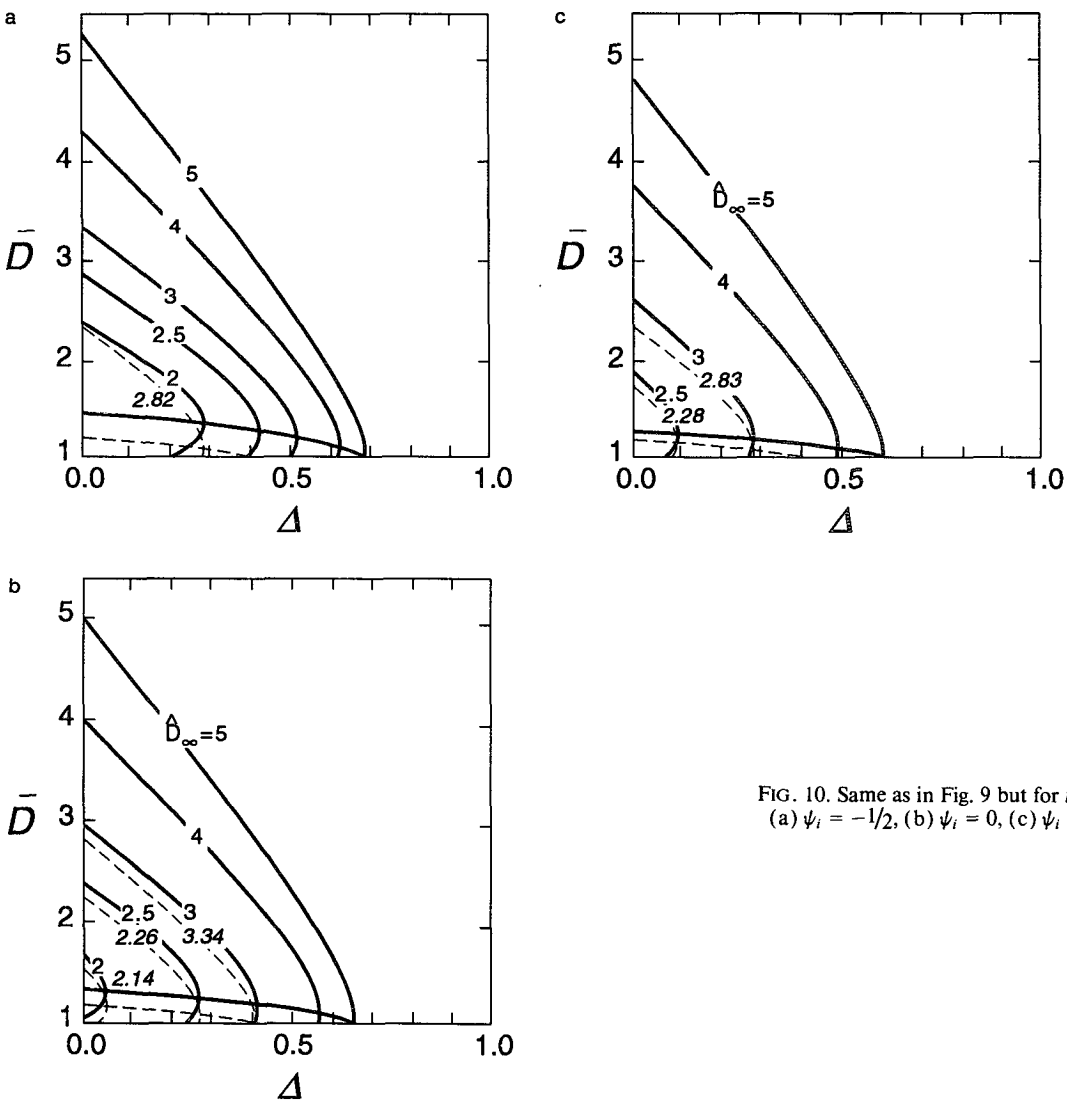

FIG. 10. Same as in Fig. 9 but for $t = 0.5$: (a) $\psi_i = -1/2$, (b) $\psi_i = 0$, (c) $\psi_i = 1/2$.

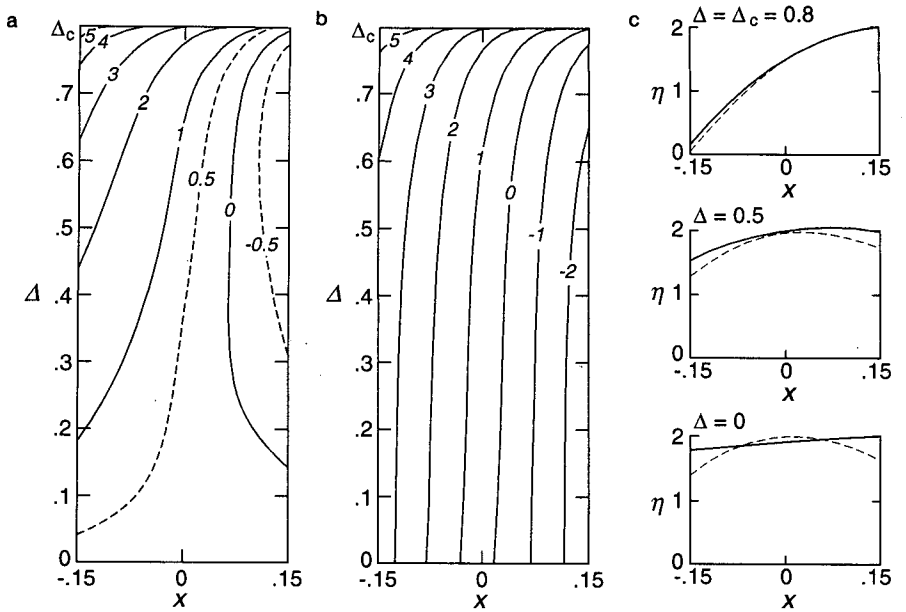

FIG. 11. (a) Velocity field for a controlled flow of constant (nonzero) potential vorticity in a channel of constant width ($t = 0.3$) that deepens upstream. The critical height is given by $\Delta_c \approx 0.8$. The flow is characterized by $\hat{D}_\infty = 10$ and $\psi_i = 1/2$. (b) Velocity field for a controlled flow described by the narrow channel–deep reservoir model. The channel geometry is the same as in (a) and $\hat{D}_\infty \approx 9.93$. (c) Depth profiles at the control section $\Delta_c \approx 0.8$, for $\Delta = 0.5$ and $\Delta = 0$. Solid lines pertain to the constant (nonzero) potential vorticity flow and dashed lines to the simplified flow.

channel equations predict a recirculation area that extends throughout the upstream basin. Again, this is due to the fact that the velocity shear has to equal $-2\hat{D}_\infty$ everywhere. Therefore, the upstream velocity structure will not, in general, resemble the one of a quiescent basin.

7. Summary and discussion

The two questions addressed in the Introduction concerned the identification of the potential depth in rotating hydraulic models for flows of constant (but nonzero) potential vorticity and the applicability of the deep reservoir–narrow channel approximation. The questions were mainly raised for practical purposes. If there are reasons to believe that the flow through a strait or over a sill is maximized, then the hydraulic theory for flows of constant (nonzero) potential vorticity provides an estimate of the transport given the geometry at the control section, the upstream distribution of the flow, together with the values of f, g', and the potential depth. Suppose that a hydrographic cross section has been taken in the upstream basin and that it demonstrates a flat interface in the interior. Using the depth (of the lower layer) in this region in the width and depth scales in section 2, it is possible to assert from Figs. 3 and 4 whether it is compatible with the hydraulic theory to identify the potential depth with the measured upstream, interior depth. The information given in Figs. 3 and 4 would also be valuable when designing laboratory experiments.

It was stated in section 2 that the flow takes on a boundary structure when the upstream basin is wide enough, leaving the interior quiescent. An alternative upstream situation for a wide basin has been presented by Killworth (1992). The velocities in the upstream reservoir in this case are small in the entire basin, a state that requires a nonuniform distribution of the potential vorticity.

In sections 4–6 the deep reservoir–narrow channel approximation was examined in detail. It was shown that in order to obtain the simplified equations, often referred to as the zero potential vorticity equations, it was necessary to assume not only that the width of the channel was small (compared to the Rossby radius of deformation based on the potential depth), but also that the depth close to and at the constriction was much smaller than the potential depth (the "high sill" approximation). The crucial parameter turned out to be the width of the channel. It was shown that for very narrow straits ($t_c < 0.1$) the maximum transport predicted by the deep reservoir–narrow channel approximation was accurate regardless of the height of the sill. This was due to the fact that $\bar{D}/\hat{D}_\infty$ appeared in the term that represents the cross-stream velocity difference, a term that is very small when the channel is narrow. When tracing the approximate solution upstream, the depth profiles follow those of a constant

(but nonzero) potential vorticity flow quite accurately as long as the channel width remains narrow. The curvature is, however, larger for the former flow, which leads to an enhanced discrepancy between the velocity profiles. The difference in the depth and velocity profiles becomes more pronounced the wider the channel gets. The problem with the simplified model is that the velocity shear is set equal to $-2\hat{D}_\infty$ and the curvature of the surface is also determined by this quantity. To keep the transport constant, the depth profile moves across the section to adjust to a widening or deepening channel. The result will finally be a separated flow or a recirculation area extending to infinity in the upstream basin. Whenever $w^2 > (1-\Delta)/2 + [(1-\Delta)^2/4 - 1/\hat{D}_\infty^2]^{1/2}$ there will always be one streamline on which $v = 0$ and $D = \hat{D}_\infty$. For the other streamlines the Bernoulli function will be made up by a lower value of the depth and a nonsmall velocity term.

The strength of the deep reservoir–narrow channel model is that it provides a good approximation of the maximum transport for a constant (nonzero) potential vorticity flow characterized by $\psi_i = 0, 1/2$. It was shown that the difference only amounts to around 20%. For these flows the agreement of the depth and velocity profiles between the two models is also good at, and close to, the control section. Away from this section the simplified model becomes increasingly inaccurate (demonstrated especially in the velocity profiles) and should be avoided.

Finally, a comment will be given on the case of a channel of parabolic cross section. When the deep reservoir–narrow channel approximation is used for this geometry, the solution to the equation corresponding to Eq. (21) may cease to exist. The reason for this behavior is that the flow cannot separate from the wall in order to maintain a constant transport since there is no distinction between the wall and the bottom. The use of the simplified model is therefore more limited for a parabolic channel than it is for a channel of rectangular cross section.

Acknowledgments. This work has been carried out with support from the Swedish Natural Science Research Council under Contract G-GU9811. Technical assistance from Deborah Taylor and John Cook is greatly appreciated.

REFERENCES

Borenäs, K. M., and P. A. Lundberg, 1988: On the deep-water flow through the Faroe Bank Channel. *J. Geophys. Res.*, **93,** 1281–1292.

——, and L. J. Pratt, 1990: Review of rotating hydraulics. *Physical Oceanography of Sea Straits,* L. J. Pratt, Ed., Kluwer, 321–341.

Gill, A. E., 1977: The hydraulics of rotating channel flow. *J. Fluid Mech.*, **80,** 641–671.

Killworth, P. D., 1992: Flow properties in rotating, stratified hydraulics. *J. Phys. Oceanogr.*, **22,** 997–1017.

Pratt, L. J., and P. A. Lundberg, 1991: Hydraulics of rotating strait and sill flow. *Annu. Rev. Fluid Mech.*, **23,** 81–106.

Whitehead, J. A., 1986: Flow of a homogeneous rotating fluid through straits. *Geophys. Astrophys. Fluid Dyn.*, **36,** 187–205.

——, 1989: Internal hydraulic control in rotating fluids—Applications to oceans. *Geophys. Astrophys. Fluid Dyn.*, **48,** 169–192.

——, A. Leetmaa, and R. A. Knox, 1974: Rotating hydraulics of strait and sill flows. *Geophys. Fluid Dyn.*, **6,** 101–125.